Since January 2020 Elsevier has created a COVID-19 resource centre with free information in English and Mandarin on the novel coronavirus COVID-19. The COVID-19 resource centre is hosted on Elsevier Connect, the company's public news and information website.

Elsevier hereby grants permission to make all its COVID-19-related research that is available on the COVID-19 resource centre - including this research content - immediately available in PubMed Central and other publicly funded repositories, such as the WHO COVID database with rights for unrestricted research re-use and analyses in any form or by any means with acknowledgement of the original source. These permissions are granted for free by Elsevier for as long as the COVID-19 resource centre remains active.

Veterinary Microbiology 271 (2022) 109491

Contents lists available at ScienceDirect

Veterinary Microbiology

journal homepage: www.elsevier.com/locate/vetmic

An influenza virus vector candidate vaccine stably expressing SARS-CoV-2 receptor-binding domain produces high and long-lasting neutralizing antibodies in mice

Yongzhen Zhao [a], Lingcai Zhao [a], Yingfei Li [a], Qingzheng Liu [a], Lulu Deng [a], Yuanlu Lu [a], Xiaoting Zhang [a], Shengmin Li [a], Jinying Ge [b], Zhigao Bu [b], Jihui Ping [a,*]

[a] MOE Joint International Research Laboratory of Animal Health and Food Safety, Engineering Laboratory of Animal Immunity of Jiangsu Province, College of Veterinary Medicine, Nanjing Agricultural University, Nanjing 210095, China

[b] State Key Laboratory of Veterinary Biotechnology, Harbin Veterinary Research Institute, Chinese Academy of Agricultural Sciences, Harbin 150069, China

ARTICLE INFO

Keywords:
Influenza virus vector
SARS-CoV-2
Influenza C virus
Receptor-binding domain
Live attenuated vaccine

ABSTRACT

Viral infectious pathogens, such as the severe acute respiratory syndrome coronavirus 2 (SARS-CoV-2) and influenza virus, can cause extremely high infection rates and mortality in humans. Therefore, it is urgent to develop an effective vaccine against coronavirus and influenza virus infection. Herein, we used the influenza virus as a vector to express the SARS-CoV-2 spike receptor-binding domain (RBD) and hemagglutinin-esterase-fusion (HEF) protein of the influenza C virus. We then evaluated the feasibility and effectiveness of this design strategy through experiments *in vitro* and *in vivo*. The results showed that the chimeric viruses could stably express the HEF protein and the SARS-CoV-2 spike RBD at a high level. BALB/c mice, infected with the chimeric virus, exhibited mild clinical symptoms, yet produced high specific antibody levels against RBD and HEF, including neutralizing antibodies. Importantly, high neutralizing antibodies could be retained in the sera of mice for at least 20 weeks. Altogether, our data provided a new strategy for developing safe and effective COVID-19 and influenza virus vaccines.

1. Introduction

Coronaviruses (CoVs), a group of enveloped viruses with a positive-sense, single-stranded RNA genome, cause severe respiratory diseases (Miller et al., 2020). Coronaviruses have caused three epidemics in the 21st century, including severe acute respiratory syndrome (SARS) in 2003, middle east respiratory syndrome (MERS), and coronavirus disease 2019 (COVID-19) (Shuai et al., 2021). The COVID-19 caused by severe acute respiratory syndrome coronavirus 2 (SARS-CoV-2) caused very high human infection rates and mortality and bring huge burdens to the global economy and human health (Zhao et al., 2022; Chen et al., 2022). As of May 21, 2022, more than 526 million cases had been reported worldwide, with 6.29 million deaths (https://www.worldometers.info/coronavirus/).

Influenza C virus (ICV) was first isolated in 1947 from a human with upper respiratory symptoms in the United States (Matsuzaki et al., 2016). This virus has been classified as a member of the Orthomyxoviridae family of enveloped and segmented negative-sense RNA viruses and influenza A, B, and D viruses. ICV commonly causes cold-like symptoms and sometimes causes lower respiratory infection, especially in children < 2 years of age (Sederdahl and Williams, 2020). After viral infection, patients often show symptoms of a cold, such as cough, fever, and fatigue (Matsuzaki et al., 2006). The hemagglutinin-esterase-fusion (HEF) glycoprotein is the counterpart of both hemagglutinin (HA) and neuraminidase (NA) in influenza A and B viruses (Wang and Veit, 2016). Although ICV outbreaks are not as widespread and are not as severe as those caused by influenza A and B virus infections, multiple etiological and serological investigations have shown that the virus is particularly widespread worldwide (Salez et al., 2014), and there is also no vaccine for ICV. Therefore, prevention of ICV is also particularly important, especially for children and adolescents.

The current pandemic of COVID-19 caused by SARS-CoV-2

* Corresponding author.
E-mail addresses: 18853858020@163.com (Y. Zhao), 2018207020@njau.edu.cn (L. Zhao), 15617938913@163.com (Y. Li), vetliuqingzheng@126.com (Q. Liu), dll980620@163.com (L. Deng), luyuanlu1212@163.com (Y. Lu), 1732767215@163.com (X. Zhang), lishengmincandy@163.com (S. Li), gejinying@caas.cn (J. Ge), buzhigao@caas.cn (Z. Bu), jihui.ping@njau.edu.cn (J. Ping).

https://doi.org/10.1016/j.vetmic.2022.109491
Received 3 March 2022; Received in revised form 2 June 2022; Accepted 6 June 2022
Available online 9 June 2022
0378-1135/© 2022 Elsevier B.V. All rights reserved.

highlights an urgent need to develop a safe, efficacious, and durable vaccine. Although many coronavirus vaccines are under development, mRNA and protein subunit vaccines are the most studied types. Virus vectors are the second most commonly used platform for COVID-19 vaccine development, and several viral vectors have been used for research, such as adenovirus (Feng et al., 2020), vesicular stomatitis virus (VSV) (Yahalom-Ronen et al., 2020), measles virus (MEV) (Lu et al., 2021; Hörner et al., 2020), influenza A virus (IAV) (Loes et al., 2020; Koonpaew et al., 2021), oncolytic virus (Sun et al., 2021a), rabies virus (Kurup et al., 2021), Newcastle disease virus (NDV) (Sun et al., 2020a, 2021b), modified vaccinia virus Ankara (MVA) (Liu et al., 2021) and so on.

Both influenza virus and SARS-CoV-2 virus are respiratory tract viruses, resulting in pneumonia in severe cases. This study developed an influenza-based vaccine candidate expressing SARS-CoV-2 receptor-binding domain and HEF of influenza C virus to preventing both SARS-CoV-2 and ICV infection. Through the evaluation of the recombinant virus, we found that it has many remarkable characteristics, such as stability, low pathogenicity, and high antibody levels. In summary, we have developed a vaccine candidate that produces high antibody levels to HEF of influenza C virus and RBD of SARS-CoV-2, including neutralizing antibodies for SARS-COV-2, and provided a new strategy for designing vector-based vaccine against both influenza virus and SARS-CoV-2.

2. Materials and methods

2.1. Cells

Human embryonic kidney (HEK293T) cells and African green monkey kidney (Vero E6) cells were cultured in Dulbecco's Modified Eagle's Medium (DMEM; Gibco) containing 10 % fetal bovine serum (FBS; Gibco), 0.2 % $NaHCO_3$, 100 μg/ml streptomycin, and 100IU/ml penicillin (Gibco) at 37 °C with 5 % CO_2. Madin-Darby Canine Kidney (MDCK) cells were grown in Minimum Essential Medium (MEM) containing 10 % fetal bovine serum (FBS; Sigma).

2.2. Construction of plasmids and virus rescue

(1) The full-length HA gene segment of A/Puerto Rico/8/1934 (H1N1, PR8) except the packaging signal was replaced with an open reading frame of the HEF gene of influenza C virus(C/JJ/1950) and then was inserted into the RNA polymerase I vector pHH21 (Neumann et al., 1999). All the ATGs were mutated into TTGs in the HA packaging signal region to express the HEF gene. (2) The RBD region of the Spike gene of SARS-CoV-2 (Wuhan-Hu-1) was ligated with PR8 NA stalk region sequences by a GSAGSA linker and then was inserted into the RNA polymerase I vector pHH21. (3) The PR8 HA head region was replaced with RBD and ligated by a GSAGSA linker. (4) The full-length PR8 HA segment except the packaging signal was replaced with the coding region of the second chimeric plasmid, the full-length PR8 NA segment except the packaging signal was replaced with HEF, and all the ATGs were mutated into TTGs in the HA and NA packaging signal regions. The twelve-plasmid reverse genetics system was used to generate recombinant virus (Ping et al., 2015). Two days post-transfection, culture supernatant was collected, and 0.2 ml supernatant was inoculated into 9-day-old specific-pathogen-free (SPF) embryonated chicken eggs (rPR8-$HA_{C/HEF}$-NA_{RBD}) or MDCK-HA (rPR8-HA_{RBD}) for virus propagation at 37 °C.

Virus titers were measured by 50 % tissue culture infectious doses ($TCID_{50}$) and calculated using the method of Reed & Muench.

2.3. Growth kinetics analysis

To evaluate the replication ability of recombinant virus *in vitro*, 100 $TCID_{50}$ of chimeric virus (rPR8-$HA_{C/HEF}$-NA_{RBD}) or wild-type PR8 (PR8 WT) was inoculated into 9-day-old SPF embryonated chicken eggs. The allantoic fluid of three eggs was harvested at 12, 24, 36, 48, 60, 72 and 84 h post-infection and titrated by Median tissue culture infective dose assay. Meanwhile, monolayer MDCK (rPR8-$HA_{C/HEF}$-NA_{RBD}) or MDCK-HA (rPR8-HA_{RBD}) cells were infected with viruses at a multiplicity of infection (MOI) of 0.01 and 0.1 in triplicate. The cell supernatant was harvested at 12, 24, 36, 48, 60 and 72 h post-infection and $TCID_{50}$ was determined in cell supernatants. When the viruses propagated in cells, 0.3 % BSA and 1 μg/ml TPCK-trypsin were added to DMEM.

2.4. Immunofluorescence assay

MDCK cells were seeded in glass coverslips and were inoculated at an MOI of 0.1 with the chimeric virus and PR8 WT. Thirty-six hours post-infection, the cells were washed with PBS, fixed with 4 % paraformaldehyde at room temperature for 30 min, and non-permeabilized or permeabilized with 0.1 % Triton X-100 for 15 mins. Then, the cells were washed three times with PBS and blocked with 5 % skim milk at 37 °C for 1 h. And then, the cells were washed three times and labeled with primary antibodies (mouse anti-NP monoclonal antibody and human anti-RBD polyclonal antibody) for 1 h followed by staining with secondary fluorescence antibodies (Beyotime, China). Finally, cells were stained with 4′,6-diamino-2-phenylindole (DAPI) for 10 mins and imaged under confocal microscopy (Nikon, Japan). For the tissue immunofluorescence experiment, the methods were the same as above except for antigen thermal repair with sodium citrate buffer solution.

2.5. Western Blot

Ninety-five percent of confluent MDCK cells were inoculated with the indicated virus at an MOI of 0.5. Twenty-four hours post-infection, the cells were washed with cold PBS three times and lysed with cold NP-40 lysis buffer (Beyotime, China) on ice, and the lysate was centrifuged at 12 000 revolutions per minute (RPM) for 10 mins at 4 °C and subjected to SDS-PAGE electrophoresis. Proteins in the lysates were separated by SDS-PAGE, transferred to nitrocellulose membranes, and the membrane was incubated overnight for primary antibodies and then for HRP-conjugated secondary antibodies. Finally, the membranes were incubated with enhanced chemiluminescence (ECL) reagents (Vazyme, China), and the signals were analyzed using an Amersham™ Imager 600 CCD-based chemiluminescent analyzer (GE Healthcare).

2.6. Assessment of viral pathogenicity

Female SPF BALB/c mice aged seven to eight weeks were purchased from a Shanghai Xipuer-bikai Laboratory Animal Ltd. Co. All mice were randomly divided into five groups (n = 10) and kept in individually ventilated cages. After three days of observation, the mice were anesthetized with isoflurane and then intranasally inoculated with 10^3-10^5 $TCID_{50}$/mouse of the chimeric virus.10^3 $TCID_{50}$/mouse of PR8 WT and PBS were used as positive control and negative control, respectively. The body weight change of the mice was monitored daily. Mice that lost more than 25 % of their body weight were euthanized. At day 5 post-infection, five mice in each group were euthanized with their fresh lungs harvested, and the viral RNA level of NP gene in the mice lungs was measured by RT-qPCR after homogenizing. The remaining lung tissue was used for HE staining and tissue immunofluorescence assay.

2.7. RT-qPCR

Total RNA was extracted from allantoic fluids, cellular supernatant, or tissue using Trizol (Vazyme, China) and performed reverse transcription (primer U12: CACACACGTCTCCGGGAGCAAAAGCAGG) using HiScript 1st Strand cDNA Synthesis Kit (Vazyme, China). Quantitative real-time PCR was then performed using the cDNAs and gene-specific primer pairs and AceQ qPCR SYBR Green Master Mix (Vazyme, China) in a Roche

LightCycler 96, according to the manufacturer's instructions using the following cycling program: 95 °C for 5 mins and 40 cycles of 95 °C for 10 s and 60 °C for 30 s. For absolute quantitative PCR, NP gene (F: TGTGTATGGACCTGCCGTAGC, R: CCATCCACACCAGTTGACTCTTG) was used to detect virus replication. The $2^{\wedge(-\Delta\Delta Ct)}$ method was used to determine the candidate genes' relative mRNA. GAPDH was used as an internal control for the detection of cytokines, and the PBS group was used as reference.

2.8. Mice vaccination

The 7–8 weeks old BALB/c mice were divided into 12 groups (n = 10) and received live virus (10^5 $TCID_{50}$ per mice) immunization using 4 alternant prime-boost (2-week interval) regimens including (i) intranasal-intranasal (*i.n.-i.n.*); (ii) intranasal-intramuscular (*i.n.-i.m.*); (iii) intramuscular- intramuscular (*i.m.-i.m.*); (iv) intramuscular- intranasal (*i.m.-i.n.*) routes. Five mice in each group were euthanized randomly one week after each immunization, and their sera, splenic lymphocytes, and lungs were harvested.

2.9. Isolation of splenic lymphocytes, bronchoalveolar lavage fluid, and intranasal rinse

Mice were euthanized and soaked in 75 % alcohol for 1–2 min for sterilization. The spleen was harvested, and non-splenic tissue was clipped and rinsed in serum-free RPMI Medium 1640 (Gibco). After grinding on a 200-mesh screen, the spleen cells were collected in dishes. The precipitated cells were collected after centrifugation at 800 *g* for 5 mins. Then, the red blood cells were lysed with red blood cell lysis solution and centrifuged at 800 *g* for 5 mins. Finally, the cells were rinsed in serum-free RPMI Medium 1640 and serum-containing RPMI Medium 1640. After one more round of centrifugation, the cells were resuspended in serum-containing RPMI Medium 1640. After cell counting, it was used for subsequent experiments.

For isolation of bronchoalveolar lavage fluid and intranasal rinse, we used 800ul PBS to rinse the broncho-alveoli of mice 3 times, and 300ul PBS to repeatedly rinse the nasal cavity of mice 3 times. After centrifugation, the supernatant was taken for subsequent experiments.

2.10. Determination of $CD4^+$ and $CD8^+$ T cell subsets

For determination of $CD4^+$ and $CD8^+$ T Cell Subsets, 10^7 lymphocytes were collected in the centrifuge tube, and the cell surface was stained with Fc blocking (BioLegend, USA), then incubated with CD3-FITC, CD4-PE/Cy7 (Proteintech, China) and CD8-PE (BioLegend, USA) for 30 min without light. The cell population was then analyzed by flow cytometry.

2.11. Enzyme-linked immunosorbent assay (ELISA)

Both RBD and HEF proteins were previously expressed by prokaryotes and purified. Ninety-six-well plates were first coated with 100 μl of highly purified protein (3 μg/ml, in 50 mM Na_2CO_3 buffer, pH 9.6) per well at 4 °C overnight and then blocked with Bovine Serum Albumin (BSA, 1 % W/V in PBS, 100 μl/well) at 37 °C for 2 h. Subsequently, individual sera samples were tested for RBD- or HEF-specific Ab on antigen-coated plates. Briefly, sera samples were 2-fold serially diluted and added to protein-coated wells (100 μl/well). After 2 h of incubation at room temperature, the plates were washed three times with phosphate-buffered saline containing 0.05 % Tween (PBST), followed by incubation with 100 μl of horseradish peroxidase (HRP)-conjugated secondary Abs (Sigma) at a dilution of 1:15 000 for 1 h. The plates were washed, developed with 100 μl of SureBlue™ TMB 1-Component Microwell Peroxidase Substrate (Fisher Scientific, Catalog No.50–674–93), and stopped by 100 μl of H_2SO_4 (2 mol/L). Optical densities (OD) at 450 nm were determined by a BioTek microplate reader. 2.1 times the OD_{450} mean value of the blank control was used as the cut-off value.

2.12. Determination of neutralizing antibodies levels against SARS-CoV-2

The levels of neutralizing antibodies in the sera of mice were tested by the Anti-SARS-CoV-2 Neutralizing Antibodies ELISA Kit (Vazyme, China). In the first step of the reaction, the samples were pre-incubated with the HRP-conjugate antigen in a 96-well plate and then transferred into the hACE2-coated plates. The HRP-conjugate antigen unbound with the neutralizing antibodies would bind with hACE2. The plates were washed, developed with TMB substrate solution and stopped by stop solution. Optical densities (OD) at 450 nm were determined by a BioTek microplate reader. The neutralizing antibodies inhibition rate of the samples was calculated as follows: inhibition rate = [1-OD_{450}(sample)/OD_{450}(negative control)] * 100 %. If the inhibition rate is less than 20 %, there is no neutralizing antibodies in the sera.

Pseudotyped virus (PV) with the green fluorescent protein (GFP) displaying the full-length spike protein of SARS-CoV-2 (Wuhan strain) was used as described previously (Liu et al., 2017). Briefly, mouse sera were heat-inactivated at 56 ℃ for 30 min before use in the assay. The sera samples were two-fold serially diluted in DMEM supplemented with 2 % FBS in sextuplicate and incubated with 100 $TCID_{50}$ PV at 37 ℃ for 1 h. Vero E6 (3×10^5 cells) were suspended in 100 μl DMEM supplemented with 10 % FBS and then added into each well. The plate was incubated at 37 ℃, 5 % CO2. The green fluorescence signal was observed and recorded after 36 h. The titer of neutralizing antibodies is defined as the reciprocal of the highest dilution. No expression of GFP in cell well was considered positive, while expression of GFP was considered negative. The number of negative and positive wells corresponding to each dilution of sera was recorded. The serum neutralizing antibodies titers were calculated according to the Reed-Muench method.

2.13. Statistical analysis

Flow cytometry data were analyzed using Flow Jo, version 10 (Tree Star, Inc.). The data were shown as mean ± SEM, and unless otherwise indicated, all the presented data are representative results of at least three independent repeats. Statistical analysis was performed with Prism 8 (GraphPad), and the statistics were analyzed by a two-tailed Student's t-test as indicated. Differences considered to be significant at $P < 0.05$ were indicated by *, those at $P < 0.01$ were indicated by **, those at $P < 0.001$ were indicated by ***, those at $P < 0.0001$ were indicated by ****, ns, no significance.

3. Results

3.1. Generation of recombinant influenza virus expressing SARS-CoV-2 RBD in HA or NA segment

RNA viruses, especially segmented RNA viruses, have limited genetic capacity. We selected the receptor-binding domain of SARS-CoV-2 spike protein as a candidate gene for inserting the influenza virus genome because RBD is small in size (~200 aa) and folds autonomously. Additionally, RBD induces the body to produce the most potent neutralizing antibodies against SARS-CoV-2. Here we constructed several influenza viruses expressing RBD. Firstly, to generate the chimeric influenza genes that encodes the membrane-anchored RBD, the RBD region was fused with the transmembrane domain and cytoplasmic tail of PR8 NA. Besides, the HEF of ICV has the functions of HA and NA of IAV, enabling the normal replication of NA- or HA-deficient viruses, and ICV is also a pathogen with infection risk to humans. So, we constructed a chimeric vector that the open reading frame of the HEF gene was inserted between the PR8 HA gene packaging signals, and all ATGs in packaging signal regions were mutated to TTGs for the precise expression of the HEF gene. Subsequently, chimeric viruses named rPR8-$HA_{C/HEF}$-NA_{RBD}

were generated using the twelve-plasmid reverse genetics system (Fig. 1B). In addition, the wild-type PR8 virus was successfully rescued as a positive control (Fig. 1A). Secondly, the PR8 HA head region was replaced with RBD and ligated by a GSAGSA linker, and rPR8-HA_{RBD} was rescued with other PR8 segments (Fig. 1C). As reported in previous literature, the virion surface of the influenza A virus has approximately 300–400 hemagglutinin trimer proteins and 40–50 neuraminidase tetramer proteins (Harris et al., 2006), although the numbers of each protein vary between the different subtypes. The ratio of HA and NA is 4–14:1 (Zheng et al., 2020). To increase the proportion of RBD protein on the viral surface, the coding region of the sixth segment in Figure B was inserted between the HA gene packaging signals. Except for the packaging signal, the full-length PR8 NA segment was replaced with HEF. All ATGs in HA and NA packaging signal regions were mutated to TTGs (Fig. 1D). Unfortunately, the chimeric virus failed to rescue after several attempts. So, we focused on the two chimeric viruses, rPR8-$HA_{C/HEF}$-NA_{RBD} and r-PR8-HA_{RBD} in the following studies.

3.2. Two chimeric influenza viruses replicated efficiently in SPF embryonated chicken eggs or cells but showed attenuated replication

To compare the growth characters of chimeric viruses with the wild-type PR8, we inoculated embryonated chicken eggs (100 $TCID_{50}$/egg) and infected MDCK or MDCK-HA cells with the viruses at different MOI (0.1 and 0.01). The data showed that chimeric viruses had a slower and attenuated growth capacity than PR8 WT, which is caused by changing viral surface protein structure. The peak yield of rPR8-$HA_{C/HEF}$-NA_{RBD} reached 1.66×10^7 $TCID_{50}$ /ml in chicken eggs and 3.63×10^5 $TCID_{50}$/ml in MDCK cells. The vital titers of rPR8-HA_{RBD} were 7.76×10^5 and 3.16×10^5 $TCID_{50}$/ml at 24 and 48 h post-infection in MOI= 0.1 and MOI= 0.01 MDCK-HA infection groups, respectively, which were 6.8 and 11.5 times lower than PR8 WT (Fig. 2). Thus, the replicative ability of two chimeric viruses was attenuated in mammalian cells and embryonated chicken eggs.

3.3. RBD could be highly expressed in virus-infected cells

To detect the SARS-CoV-2 RBD protein expression level of two chimeric viruses-infected cells, we first detected the expression of RBD protein in virus-infected cells by Immunofluorescence assay. As we expected, most of the MDCK or MDCK-HA cells infected with chimeric viruses expressed both NP and RBD proteins (Fig. 3A), which indicated that almost all virus-infected cells expressed RBD protein, and viruses could express RBD protein. Moreover, we examined the expression of the RBD protein in virus-infected cells by Western blot analysis. The result similarly demonstrated that the RBD protein was expressed in both rPR8-$HA_{C/HEF}$-NA_{RBD} and rPR8-HA_{RBD} infected cells (Fig. 3B).

3.4. RBD could be detected on the surface of infected cells and assembled into the chimeric virus virions

Influenza viruses express two surface glycoproteins, the hemagglutinin and neuraminidase. During the assembly of progeny viral particles, they are recruited to the host cell membrane where it associates with lipids and other viral proteins. This study cloned the RBD into the HA or NA gene segment to replace the HA/NA head domain. Ideally, we expected the RBD domain could be recruited to the cell membrane and then integrated into the virions. So, we next determined whether cells

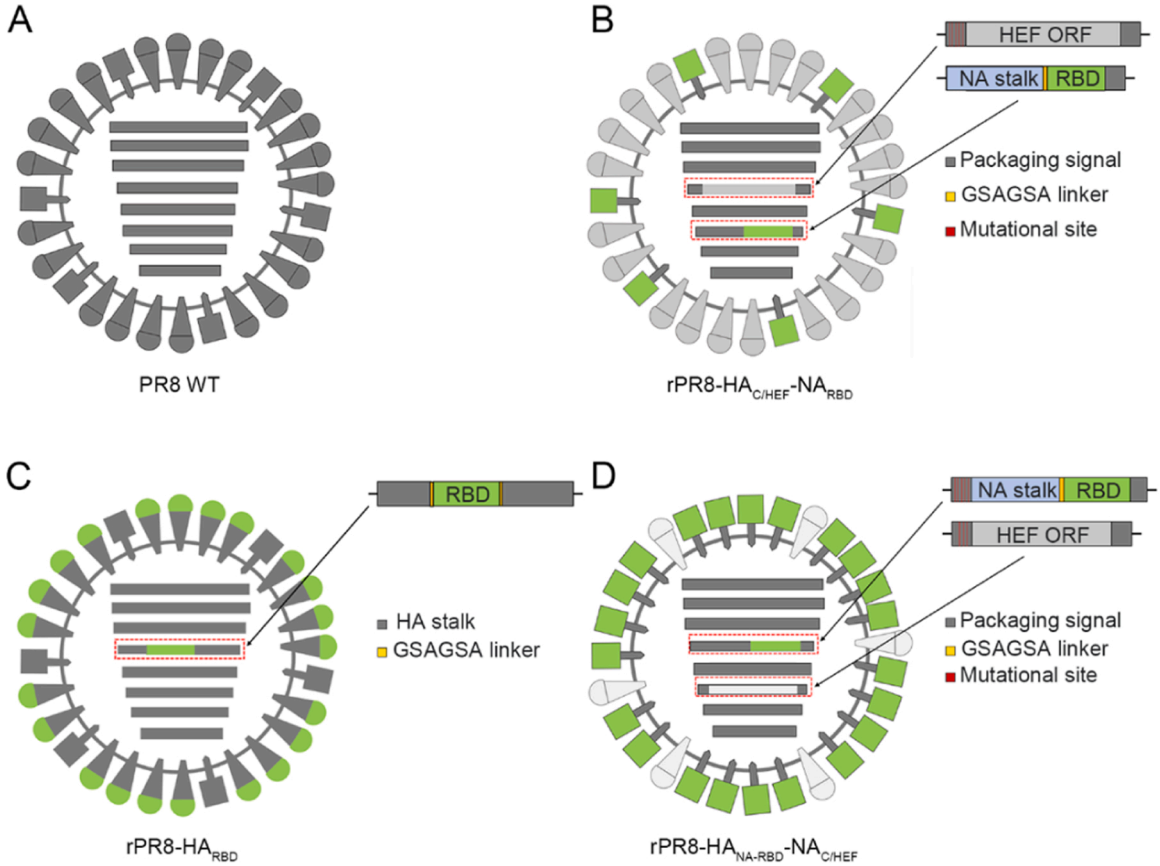

Fig. 1. The diagram of the recombinant viruses in this study. (A) Viral structure of wild-type PR8. (B-D) Strategy for insertion of SARS-CoV-2 RBD to influenza genome. The red lines represent the mutation sites, where ATGs have been mutated to TTGs. The yellow bars represent GSAGSA linker. For panel B and D, the dark gray bars at each end of the HA and NA genes represent influenza packaging signals. For panel C, the dark gray represents the packaging signal and stalk region of HA. (For interpretation of the references to colour in this figure legend, the reader is referred to the web version of this article.)

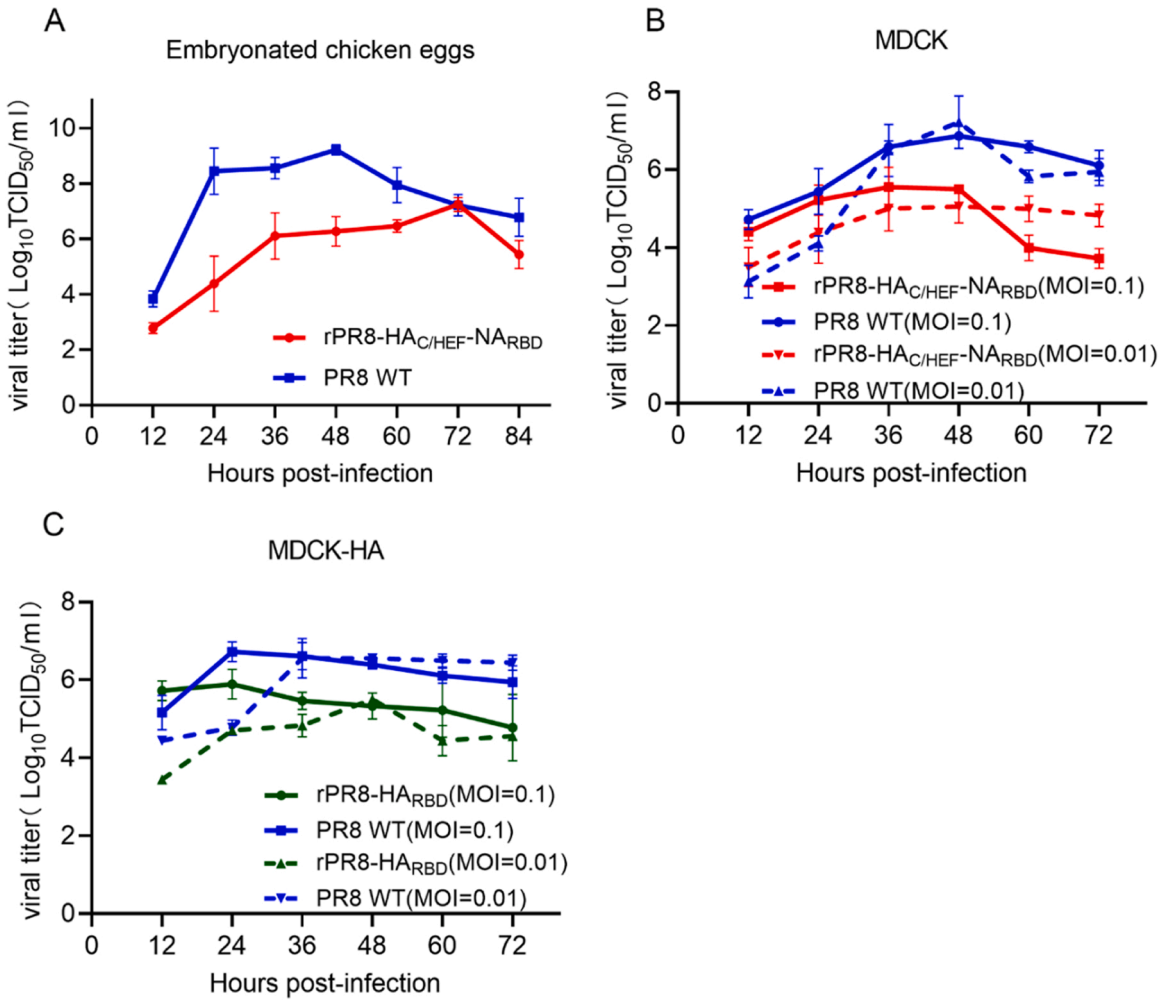

Fig. 2. Growth kinetics of chimeric viruses. (A) Growth kinetics of rPR8-$HA_{C/HEF}$-NA_{RBD} and PR8 WT in embryonated chicken eggs. (B) Growth kinetics of rPR8-$HA_{C/HEF}$-NA_{RBD} and PR8 WT in MDCK cells at MOI of 0.01 and 0.1. (C) Growth kinetics of rPR8-HA_{RBD} and PR8 WT in MDCK-HA cells at MOI of 0.01 and 0.1. Data were geometric mean titers (GMT) ± SD from n = 3 biologically independent experiments.

infected with chimeric viruses expressed RBD on their surface. To this end, viruses-infected cells were fixed but non-permeabilized treatment and then probed with anti-spike RBD antibody at 36 h post-infection. The confocal images showed that the RBD protein was localized on the surface of infected cells (Fig. 4A). To further confirm whether the RBD could also be found in newly assembled virions, we concentrated and purified the virus using sucrose density gradient centrifugation and then the purified viruses were examined by Western blot. As expect we detected RBD protein's presence in purified virions (Fig. 4B). Therefore, the above results indicated that the RBD protein was incorporated into the two chimeric virus virions.

3.5. Genetic stability of the RBD expressing viruses

For RNA viruses, the foreign genes are extremely easy to lose or mutate (Froggatt et al., 2021). Therefore, we passaged rPR8-$HA_{C/HEF}$--NA_{RBD} and rPR8-HA_{RBD} in embryonated chicken eggs (100 $TCID_{50}$/egg) or cells (MOI=0.01) respectively, to evaluate the genetics stability of the chimeric viruses. The gene amplification data showed that the RBD gene appeared to be stably maintained in embryonated chicken eggs and cells passaged the chimeric virus for at least 10 passages (Fig. 5A). In addition, to ensure that the RBD gene did not acquire terminational mutations to normally express the RBD protein during serial passages, we assessed the protein expression of the tenth passaged chimeric viruses. And we observed the RBD could be normally and largely expressed in passaged viruses (Fig. 5B). These findings further suggested the RBD gene could be stably existed and expressed in the chimeric viruses.

3.6. The pathogenicity of rPR8-$HA_{C/HEF}$-NA_{RBD} was attenuated in BALB/c mice

Compared with the tenth generation of rPR8-$HA_{C/HEF}$-NA_{RBD}, the tenth generation of rPR8-HA_{RBD} showed the lower expression level of RBD with the same MOI (Fig. 5B) and it depends on exogenous HA-expressing cell line. In addition, rPR8-$HA_{C/HEF}$-NA_{RBD} virus can also express HEF of ICV, so we selected the rPR8-$HA_{C/HEF}$-NA_{RBD} for the further tests. As the live attenuated vaccines must not be highly pathogenic to the immunization target, we intranasally *(i.n.)* infected 8-week-old female BALB/c mice with rPR8-$HA_{C/HEF}$-NA_{RBD} at a dose from 1×10^3 to 1×10^5 $TCID_{50}$ per mice to evaluate the virulence of the chimeric virus in mice model. The body weight change and survival data indicated that, mice infected with low-dose PR8 WT experienced a severe loss of body weight and had a 20 % survival rate. In contrast, none of the mice infected with the rPR8-$HA_{C/HEF}$-NA_{RBD} died and lost body weight (Fig. 6A and B). On day 5 post-infection, five mice in each group were euthanized, and lungs were collected for viral titration. The results showed that both rPR8-$HA_{C/HEF}$-NA_{RBD} and PR8 WT could efficiently replicate in mouse lungs. And the number of viral genome copies of the chimeric virus in mice lungs showed an infection dose-dependent (Fig. 6C and D). Histopathological analysis showed that PR8 WT

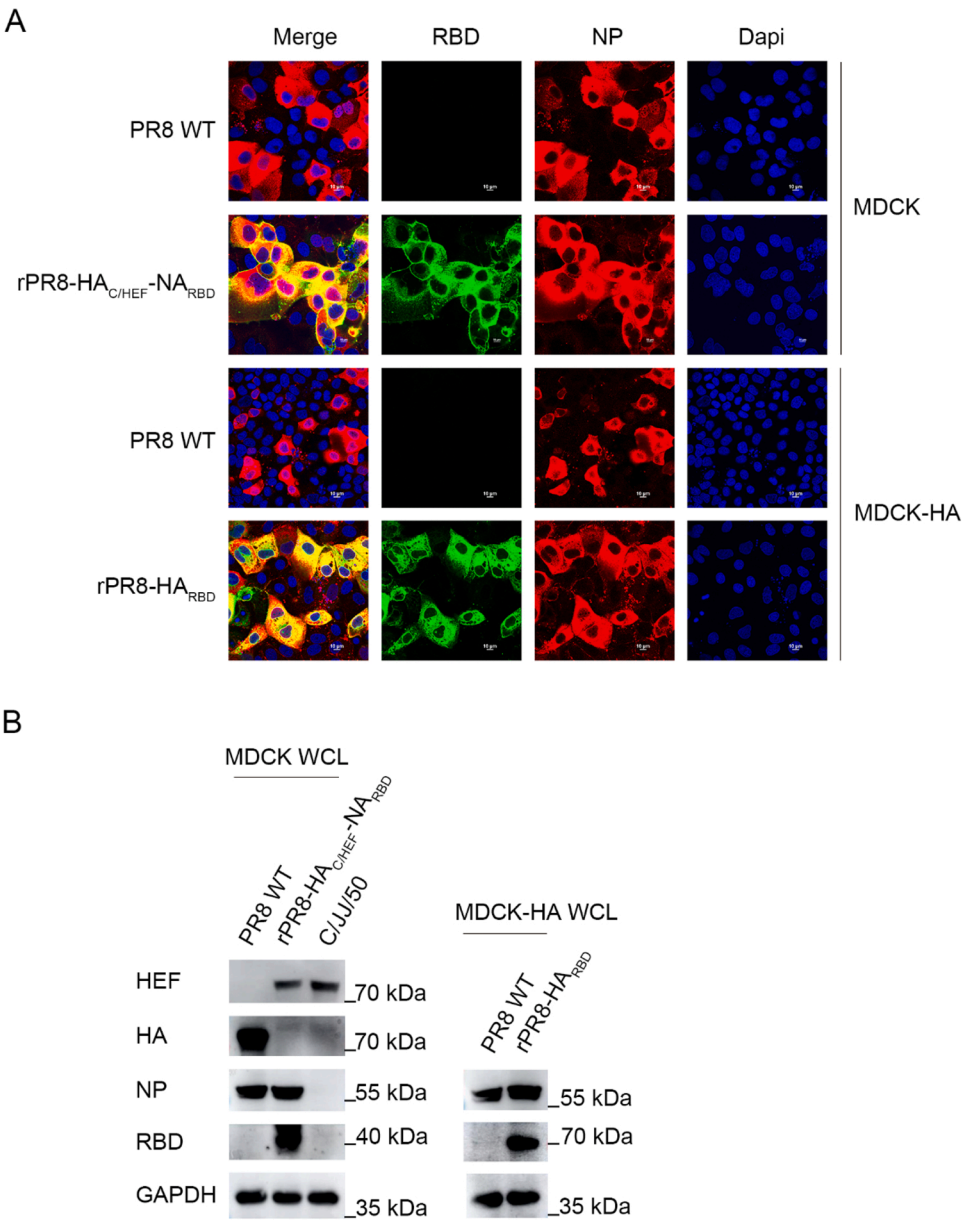

Fig. 3. The expression of SARS-CoV-2 RBD and influenza viral proteins in chimeric virus infected cells. (A) Immunofluorescence images of MDCK or MDCK-HA cells infected with rPR8-HA$_{C/HEF}$-NA$_{RBD}$, rPR8-HA$_{RBD}$ or PR8 WT. Cells were infected with viruses at MOI= 0.1. At 36 h post-infection, RBD and NP proteins were examined using a human anti-RBD monoclonal antibody or a mouse anti-NP monoclonal antibody, respectively. (B) Expression of the RBD protein in rPR8-HA$_{C/HEF}$-NA$_{RBD}$ or rPR8-HA$_{RBD}$ infected cells. Cells were infected with viruses at MOI= 0.5. At 24 h post-infection, RBD protein was examined by western blot analysis.

induced typical influenza-induced pneumonia in mice, and the chimeric virus caused little histopathological lung damage at 5 days post-infection, as seen in Fig. 6 D. Given this result, we increased the infection dose tenfold again. However, the mice did not lose weight, and no mice died (Fig. S1). Altogether, compared to PR8 WT, rPR8-HA$_{C/HEF}$-NA$_{RBD}$ had a significantly attenuated phenotype in mice. Thus, it has the potential of a live attenuated vaccine.

3.7. Twice intranasally immunized with rPR8-HA$_{C/HEF}$-NA$_{RBD}$ induced robust antibodies responses

To evaluate the antibodies responses in rPR8-HA$_{C/HEF}$-NA$_{RBD}$ immunized mice, BALB/c mice were immunized with the chimeric virus at a dose of 1×10^5 TCID$_{50}$ per mouse with several different inoculation strategies, as shown in Fig. 7A, and blood was taken from immunized mice at indicated time points for anti-sera isolation. The mice had developed mild lung inflammation at this dose, so the dose was not increased. Because intramuscular immunization with NDV LaSota expressing the spike proteins protects mice from challenge with a mouse-adapted SARS-CoV-2 (Sun et al., 2020b), we also immunized mice intramuscularly and tested the effect of the combination of the two ways. Mice that received phosphate buffer saline (PBS) were used as negative controls, whereas those received two doses of PR8 WT (50 TCID$_{50}$ per mouse) were used as mock-immunization controls. The antibody responses against RBD and HEF in the sera samples were determined by an enzyme-linked immunosorbent assay (ELISA). The intranasal-intranasal *(i.n.-i.n.)* and intramuscular-intranasal (*i.m.-i.n.*) groups with rPR8-HA$_{C/HEF}$-NA$_{RBD}$ had developed high RBD-specific antibody (Fig. 7B). The intranasal-intranasal (*i.n.-i.n.*) group induced a higher RBD-specific antibody level than other groups. For C/HEF-specific antibody, all boost immunization groups had high antibody levels and the differences were more significant (Fig. 6C). However, the RBD and HEF antibody levels were inconsistent in each group, which may be related to the abundance and expression levels of viral surface glycoproteins. Subsequently, we also tested the activity of neutralizing antibodies against SARS-CoV-2 RBD. Neutralizing antibodies titers in the rPR8-HA$_{C/HEF}$-NA$_{RBD}$ group were significantly higher than PBS group (Fig. 7D). The inhibition efficiency of neutralizing antibodies in mice could reach about 90 %, and the titer of neutralizing antibodies could reach

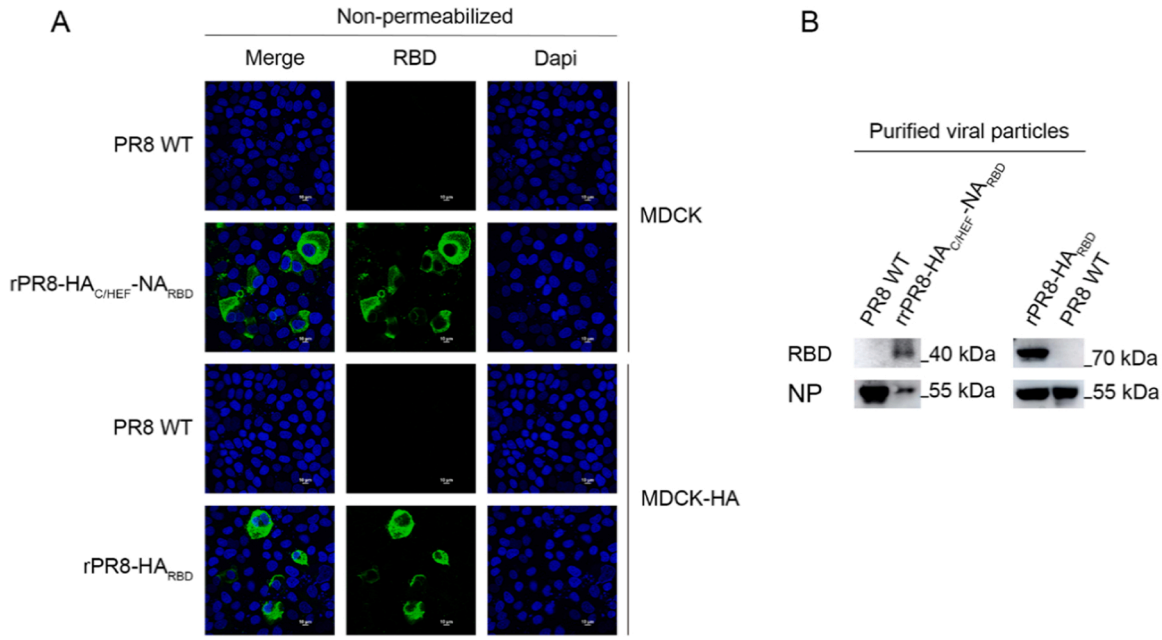

Fig. 4. The localization of RBD in viral infected cells and western blot analysis of purified viral particles. (A) Confocal microscopy displayed surface expression of a membrane anchored-RBD in infected cells. Cells were infected with viruses at MOI= 0.1. At 36 h post-infection, RBD proteins were examined using a human anti-RBD monoclonal antibody. The cells were not permeabilized before antibodies incubation. (B) Western blot analysis. The viruses were concentrated by sucrose density gradient centrifugation and then subject to SDS-PAGE electrophoresis and western blot.

9.3 log2. Therefore, it could be considered that rPR8-HA$_{C/HEF}$-NA$_{RBD}$, as a potential vaccine, could effectively produce neutralizing antibodies. In addition, mucosal immune responses in mice were evaluated. Although the results showed that OD_{450} nm could be enhanced, the difference was small and there were individual differences, which could not achieve the desired effect. (Fig. 7E, F, G, and H).

3.8. *rPR8-$_{HAC/HEF}$-NA$_{RBD}$ virus did not cause an imbalance of CD4$^+$/CD8$^+$ lymphocytes and cytokine storm*

It has been reported that total lymphocyte counts were significantly lower in patients with H1N1 pneumonia than the control group and the CD4$^+$/CD8$^+$ T lymphocytes ratio was significantly lower in the severe pneumonia group than the moderate pneumonia and control (Kim et al., 2011). To evaluate whether the live rPR8-HA$_{C/HEF}$-NA$_{RBD}$ immunization could cause the above issue, we next detected the number of CD3$^+$CD4$^+$ and CD3$^+$CD8$^+$ lymphocytes, and the proportion of two T lymphocytes in chimeric virus immunized mice by flow cytometry. The results showed that the lymphocyte counts (here, only the intranasal inoculation groups were shown) and the proportion of CD4$^+$/CD8$^+$ lymphocytes were slightly decreased compared with the PBS group (Fig. S2A and B), but there was no significant difference between the experimental group and PBS group. Abnormal cytokine storms play an important role in the pathogenesis and disease severity of the influenza A virus (Gu et al., 2019). Thus, we determined whether rPR8-HA$_{C/HEF}$-NA$_{RBD}$ vaccination produced cytokine storms in mice lungs and spleens. As shown in Fig. S2C and D, the mRNA levels of cytokines increased slightly. Among them only IFN-γ mRNA levels were significantly up-regulated. Therefore, immunized mice with rPR8-HA$_{C/HEF}$-NA$_{RBD}$ did not cause an imbalance of CD4$^+$/CD8$^+$ lymphocytes. The lungs and spleens also did not produce cytokine storms. The above data suggested that the chimeric virus has more potential as a live attenuated vaccine.

3.9. *Boosted twice with rPR8-HA$_{C/HEF}$-NA$_{RBD}$ elicited durable neutralizing antibodies against SARS-CoV-2*

To further improve antibodies levels in mice model, 8-week-old female BALB/c mice were intranasally immunized with the rPR8-HA$_{C/HEF}$-NA$_{RBD}$ prime plus 2 boosts, mice that received PBS were used as controls (Fig. 8A). Sera samples were collected from the mice at 2, 4, 6, 8, 16, 18, and 20 weeks after the third immunization. The IgG antibodies responses against RBD and HEF at sixth week were tested by ELISA, and neutralizing antibodies titers were also detected. Unfortunately, there was no increase in antibodies compared with the previous second inoculation, but they were still maintained at high levels (Fig. 8B C and D). We also examined the dynamics of the RBD neutralizing antibodies. This result suggested that the prime-boost-boost strategy elicited the RBD neutralizing antibodies with considerable durability (Fig. 8E). The high level of neutralizing antibodies in immunized mice could sustain at least 20 weeks after twice boosts.

4. Discussion

Since the SARS-CoV-2 outbreak and causing huge amounts of humans to be infected, the application of viral vector systems for vaccine development against COVID-19 has received great attention. Influenza viruses are the known causative agent of a highly contagious respiratory disease among these viral vectors. Their preferred portal of entering the respiratory mucosal epithelium makes the influenza virus as an attractive viral vector for the SARS-CoV-2 vaccine development. In addition, IAV-based vector vaccines can produce bivalent vaccines: to the foreign pathogen and IAV represented by the vector (Maeda et al., 2005; Wu et al., 2010).

Here we described two engineered influenza viruses, rPR8-HA$_{C/HEF}$-NA$_{RBD}$ and rPR8-HA$_{RBD}$. The viruses stably maintained the gene encoding the RBD over multiple passages. For rPR8-HA$_{C/HEF}$-NA$_{RBD}$ virus design, we mainly utilized the dual functions of HEF protein, sparing a gene fragment (NA) for the RBD gene insertion. At the same time, the immunized body can also produce HEF antibody, which can protect the body from ICV infection. For rPR8-HA$_{RBD}$ virus generation, we replaced the head domain of HA with RBD and virus multiplied in MDCK-HA cell line. Both chimeric viruses could incorporate RBD protein into the virus particles efficiently and recruit the RBD to the membrane of the infected cells, allowing it to be easily recognized by the

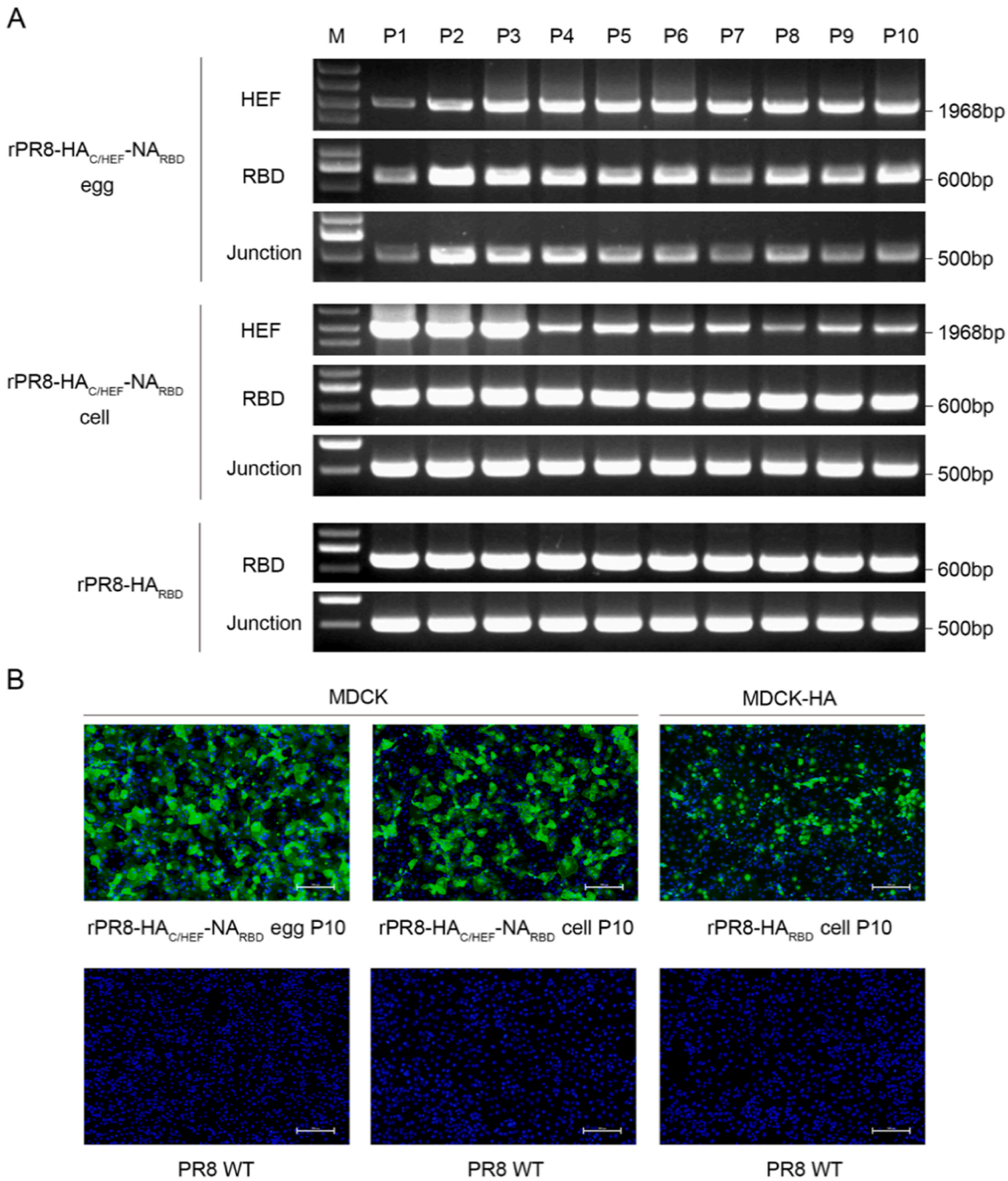

Fig. 5. Genetics stability analysis. (A) Stability analysis at the gene level. The rPR8-HA$_{C/HEF}$-NA$_{RBD}$ and rPR8-HA$_{RBD}$ were serially passaged in embryonated chicken eggs (100 TCID$_{50}$/egg) or cells (MOI=0.01) for 10 times. Total RNAs were extracted from the allantoic fluids or cellular supernatant. HEF fragment, RBD gene and junction of chimeric gene were amplified by PCR. (B) Stability analysis at the protein expression level. Cells were infected with the tenth-generation viruses at MOI= 0.1. At 36 h post-infection, RBD protein was examined using a human anti-RBD monoclonal antibody.

immune system and thus inducing a more effective specific immune response.

The chimeric virus we selected, rPR8-HA$_{C/HEF}$-NA$_{RBD}$ has the characteristics of high expression of RBD domain and genetic stability. And the pathogenicity study in the mice model also showed that viral infection caused undetectable body weight loss, and no mortality but high viral shedding in mice lungs. Those properties make it possible using this chimeric virus as a live attenuated vaccine candidate.

In addition to the above features, rPR8-HA$_{C/HEF}$-NA$_{RBD}$ also has many advantages over traditional inactive vaccines. As a live attenuated vaccine candidate, an influenza virus-based vaccine candidate can be intranasally immunized to induce mucosal immunity, which may enhance the effectiveness of immune protection. Although our vaccine candidate produced sIgA in the respiratory tract of immunized mice, the combination of the vaccine with an immune adjuvant (such as CpG and CT) significantly enhanced sIgA secretion, according to previous studies (Qin et al., 2015). Most importantly, the influenza virus is an important pathogen in respiratory diseases, most people would get a flu shot each influenza season. So, in addition to preventing SARS-CoV-2 infection, the influenza vector vaccine can also produce antibodies against influenza virus infection. We demonstrated that the mice immunized with the chimeric virus produced high specific antibodies levels against HEF

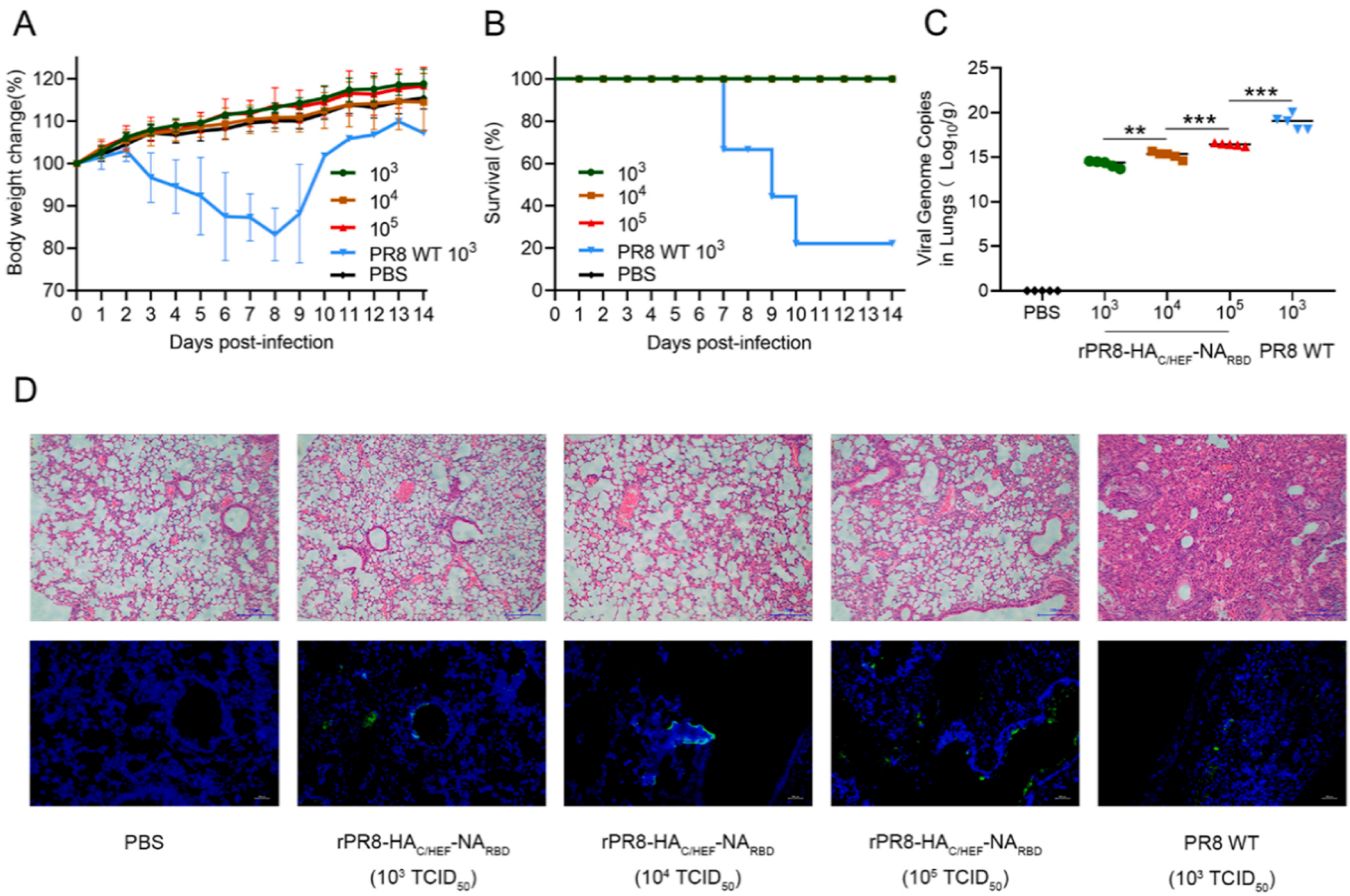

Fig. 6. Pathogenicity of rPR8-$HA_{C/HEF}$-NA_{RBD} in BALB/c mice. (A) Body weight change curves. (B) Survival curves. Mice body weight less than 75 % were considered dead and euthanized. (C) Copies of viral genomes in infected mouse lungs. At 5 days after post-infection, mice were euthanized and the lung tissues were separated and homogenized. The viral RNA levels of NP gene in the mice lungs were measured by RT-qPCR after homogenizing. (D) Pathological changes and viral loading in infected mice lungs. The lungs of infected mice were sliced and the pathological changes of the lungs were assessed by HE staining, and viral load was assessed by IFA.NP protein was detected using a mouse anti-NP monoclonal antibody.

and RBD by ELISA, suggesting that the vaccine candidate could protect against influenza C virus and SARS-CoV-2. Competitive ELISA proved that the sera of immunized mice could effectively antagonize the binding of hACE2 and RBD, and SARS-CoV-2 pseudotyped virus neutralization assay also proved that the neutralizing antibodies titers were high, which might attenuate the novel Coronavirus invasion. Previous literature reported that after influenza virus infection, the host appeared immune disorder, causing damage of organism, such as the imbalance of the $CD4^+/CD8^+$ lymphocytes ratio and the cytokine storm (Kim et al., 2011; Phung et al., 2011). Finally, we demonstrated that the $CD4^+/CD8^+$ lymphocytes ratio and cytokine mRNAs did not significantly change after live virus immunization, and there was no significant difference from the PBS group.

Otherwise, there are also undeniable drawbacks to our work. First, due to the limitation of experimental conditions, we did not perform the live SARS-CoV-2 virus challenge experiments. We will seek a high-level biosafety laboratory to carry out this part work in future. But, in this study, we tested neutralizing antibodies in mice, which could reflect the vaccine candidate's effect. Second, the influenza C virus can also infect humans, but its outbreak is pretty rare, and ICV is not as mainstream as the influenza A and B virus, which reduces its significance. But ICV is particularly prone to outbreaks in children and adolescents, which may be welfare for children to be vaccinated against these two pathogens. Third, we used the A/Puerto Rico/8/1934 virus as a backbone to generate the chimeric virus, and it is unknown whether pre-existed antibodies induced by PR8 backbone-based seasonal flu vaccines could disturb the immunity of our live vaccine candidate. According to previous studies, different influenza virus surface protein had a significant impact on virus-vector vaccines, revealing a possibility to evade the anti-vector immunity by replacing the surface proteins with those derived from an antigenically distinct influenza strain (Wang et al., 2021). For the immunity against IAV after the prime, we can change the backbone of IAV to the second dose of vaccine. In addition, we also noted that the PR8 backbone might appear gene recombination with other natural strains during immunization. But we are currently in the initial stages of vaccine development. In future work, we can replace the packaging signal with the bat influenza virus, which has been shown no recombination between strains under experimental conditions (Yang et al., 2017). Of course, we can also use the backbone of an approved cold-adapted strain.

Before the preparation of this manuscript, Andrea N. et al. incorporated a membrane-anchored form of the SARS-CoV-2 spike receptor-binding domain (RBD) in place of the neuraminidase (NA) coding sequence in an influenza virus, named ΔNA(RBD)-Flu virus (Loes et al., 2020). Surapong. et al. described a single-cycle influenza virus-based SARS-CoV-2 vaccine (scPR8-RBD-M2) that utilizes the chimeric gene encoding 2 A peptide-based bicistronic protein cassette of the SARS-CoV-2 receptor-binding domain (RBD) and influenza matrix 2 (M2) protein (Koonpaew et al., 2021). Their works are worth learning for our research. A single-dose intranasal inoculation of mice with ΔNA (RBD)-Flu virus elicits sera neutralizing antibodies titers against SARS-CoV-2 comparable to those observed in humans following natural infection. Mice inoculated with scPR8-RBD-M2 also elicited robust mucosal and cell-mediated immunity, and the mouse sera exhibited

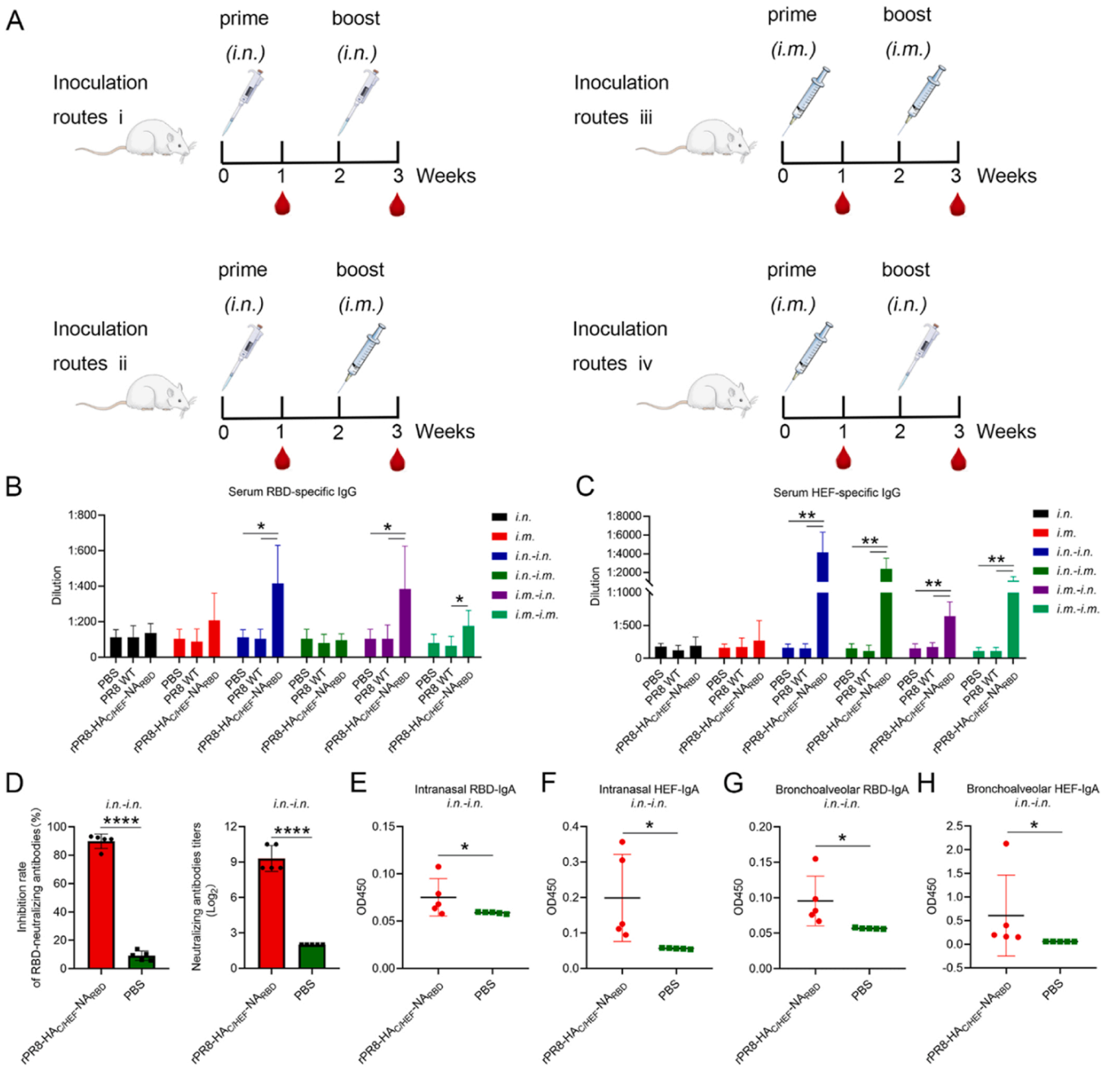

Fig. 7. Immunogenicity of rPR8-HA$_{C/HEF}$-NA$_{RBD}$ in BALB/c mice. (A) Live virus immune strategies. BALB/c mice (n = 10) were inoculated intramuscularly (*i.m.*) or intranasally (*i.n.*) with PBS, 10^5 TCID$_{50}$ of rPR8-HA$_{C/HEF}$-NA$_{RBD}$ or 50 TCID$_{50}$ of PR8 WT. 2 weeks later, mice were boosted with same dose. Samples were collected at week 1 and 3 for antibodies detection. (B) Measurement of the SARS-CoV-2 RBD-specific IgG antibody by ELISA. RBD protein was used as the coating antigen for the ELISA. Dilution: The highest dilution of antibody that can be detected. (C) Measurement of the influenza C virus HEF-specific IgG antibody by ELISA. HEF protein was used as the coating antigen for the ELISA. Dilution: The highest dilution of antibody that can be detected. (D) Measurement of SARS-CoV-2 specific neutralizing antibodies. Left: The inhibition rate of neutralizing antibodies was determined by competitive ELISA. Right: Titers of neutralizing antibodies of mice sera against Wuhan-PV. (E and G) Measurement of the SARS-CoV-2 RBD-specific IgA antibody by ELISA. (F and H) Measurement of the influenza C virus HEF-specific IgA antibody by ELISA.

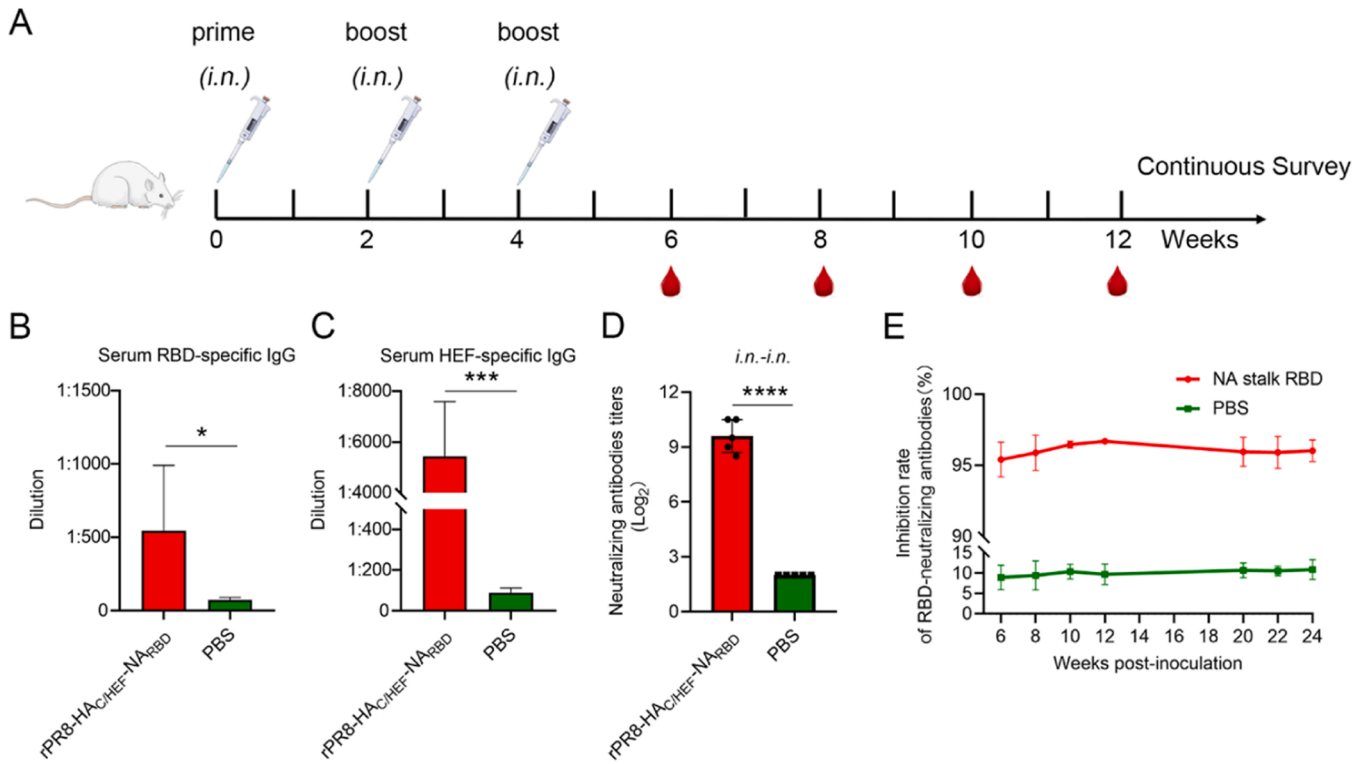

Fig. 8. Immunogenicity of mice inoculated intranasally with rPR8-$HA_{C/HEF}$-NA_{RBD} three times. (A) Live virus immune strategies. BALB/c mice (n = 5) that were intranasally inoculated with PBS or 10^5 $TCID_{50}$ of rPR8-$HA_{C/HEF}$-NA_{RBD} , and boosted twice with two weeks intervals. PBS group was used as negative control. (B) Measurement of SARS-CoV-2 RBD-specific antibody by ELISA. Dilution: The highest dilution of antibody that can be detected. (C) Measurement of influenza C virus HEF-specific antibody by ELISA. Dilution: The highest dilution of antibody that can be detected. (D) Titers of neutralizing antibodies of mice sera against Wuhan-PV. (E) Monitoring the duration of SARS-CoV-2 neutralizing antibodies in mice after three immunization.

neutralizing activity against pseudotyped viruses bearing SARS-CoV-2 spikes from various variants. However, none of them perform experiments to examine the durability of these titers over longer timeframes. Unlike their studies, rPR8-$HA_{C/HEF}$-NA_{RBD} elicited high and durable neutralizing antibodies. In addition, ΔNA(RBD)-Flu virus did not be examined the stability of the gene encoding the RBD in detail, and scPR8-RBD-M2 must require HA stable expression cells. Thus, we specifically demonstrated the genetic stability at least 10 passages and chose the multi-cycle chimeric virus for research.

5. Conclusion

We have established a potential influenza vector vaccine platform against SARS-CoV-2 and influenza virus infection. The chimeric virus had properties of stable gene expression, cell membrane incorporation, and low pathogenicity in mice. After being immunized with the live attenuated virus, the mice produced high specific antibody levels and neutralizing antibodies level against SARS-CoV-2. In addition, the neutralizing antibodies could last 20 weeks at least after twice boosts. Therefore, the chimeric virus we generated in this study had an excellent potential to be developed as a vaccine candidate against the influenza virus and SARS-CoV-2 infection.

Ethics statement

The animal study was reviewed and approved by the Nanjing Agricultural University Experimental Animal Welfare Ethics Committee with the approval ID is SYXK2017-0007.

Declaration of Competing Interest

The authors declare no conflict of interest.

Acknowledgments

This work was supported by National Key Research and Development Program of China (Grant number: 2021YFD1800205), National Natural Science Foundation of China (Grant number: 31772775) and the State Key Laboratory of Veterinary Biotechnology (Grant number: SKLVBF202103). We thank Prof. Yoshihiro Kawaoka (University of Wisconsin-Madison) for the gifts of the pHH21 and pCAGGS vectors.

CRediT authorship contribution statement

Yongzhen Zhao: Conceptualization, Writing – original draft, Visualization, Supervision. **Lingcai Zhao:** Writing – review & editing. **Yingfei Li:** Writing – review & editing. **Qingzheng Liu:** Visualization. **Yuanlu Lu:** Writing – review & editing. **Xiaoting Zhang:** Writing –

review & editing. **Shengmin Li:** Writing – review & editing. **Jinying Ge:** Supervision. **Zhigao Bu:** Supervision. **Jihui Ping:** Conceptualization, Project administration, Funding acquisition. All authors have read and agreed to the published version of the manuscript.

Appendix A. Supporting information

Supplementary data associated with this article can be found in the online version at doi:10.1016/j.vetmic.2022.109491.

References

Chen, N., et al., 2022. Virus-host interaction networks as new antiviral drug targets for IAV and SARS-CoV-2. Emerg. Microbes Infect. 1–56.

Feng, L., et al., 2020. An adenovirus-vectored COVID-19 vaccine confers protection from SARS-COV-2 challenge in rhesus macaques. Nat. Commun. 11 (1), 4207.

Froggatt, H.M., 2021. Influenza A virus segments five and six can harbor artificial introns allowing expanded coding capacity. PLoS Pathog. 17 (9), e1009951.

Gu, Y., et al., 2019. Role of the Innate Cytokine Storm Induced by the Influenza A Virus. Viral Immunol. 32 (6), 244–251.

Harris, A., et al., 2006. Influenza virus pleiomorphy characterized by cryoelectron tomography. Proc. Natl. Acad. Sci. USA 103 (50), 19123–19127.

Hörner, C., et al., 2020. A highly immunogenic and effective measles virus-based Th1-biased COVID-19 vaccine. Proc. Natl. Acad. Sci. USA 117 (51), 32657–32666.

Kim, J.E., et al., 2011. CD4+/CD8+ T lymphocytes imbalance in children with severe 2009 pandemic influenza A (H1N1) pneumonia. Korean J. Pedia 54 (5), 207–211.

Koonpaew, S., et al., 2021. A single-cycle influenza A virus-based SARS-CoV-2 vaccine elicits potent immune responses in a Mouse Model. Vaccine 9, 8.

Kurup, D., et al., 2021. Inactivated rabies virus vectored SARS-CoV-2 vaccine prevents disease in a Syrian hamster model. PLoS Pathog. 17 (3), e1009383.

Liu, R., et al., 2021. One or two injections of MVA-vectored vaccine shields hACE2 transgenic mice from SARS-CoV-2 upper and lower respiratory tract infection. Proc. Natl. Acad. Sci. USA 118, 12.

Liu, R.Q., et al., 2017. Newcastle disease virus-based MERS-CoV candidate vaccine elicits high-level and lasting neutralizing antibodies in Bactrian camels. J. Integr. Agric. 16 (10), 2264–2273.

Loes, A.N., 2020. Attenuated influenza virions expressing the SARS-CoV-2 receptor-binding domain induce neutralizing antibodies in mice. Viruses 12, 9.

Lu, M., 2021. A safe and highly efficacious measles virus-based vaccine expressing SARS-CoV-2 stabilized prefusion spike. Proc. Natl. Acad. Sci. USA 118, 12.

Maeda, Y., 2005. Live bivalent vaccine for parainfluenza and influenza virus infections. J. Virol. 79 (11), 6674–6679.

Matsuzaki, Y., 2006. Clinical features of influenza C virus infection in children. J. Infect. Dis. 193 (9), 1229–1235.

Matsuzaki, Y., 2016. Genetic lineage and reassortment of influenza C viruses circulating between 1947 and 2014. J. Virol. 90 (18), 8251–8265.

Miller, K., 2020. Coronavirus interactions with the cellular autophagy machinery. Autophagy 16 (12), 2131–2139.

Neumann, G., et al., 1999. Generation of influenza A viruses entirely from cloned cDNAs. Proc. Natl. Acad. Sci. USA 96 (16), 9345–9350.

Phung, T.T., et al., 2011. Key role of regulated upon activation normal T-cell expressed and secreted, nonstructural protein1 and myeloperoxidase in cytokine storm induced by influenza virus PR-8 (A/H1N1) infection in A549 bronchial epithelial cells. Microbiol Immunol. 55 (12), 874–884.

Ping, J., 2015. Development of high-yield influenza A virus vaccine viruses. Nat. Commun. 6, 8148.

Qin, T., 2015. CpG oligodeoxynucleotides facilitate delivery of whole inactivated H9N2 influenza virus via transepithelial dendrites of dendritic cells in nasal mucosa. J. Virol. 89 (11), 5904–5918.

Salez, N., 2014. Influenza C virus high seroprevalence rates observed in 3 different population groups. J. Infect. 69 (2), 182–189.

Sederdahl, B.K., Williams, J.V., 2020. Epidemiology and clinical characteristics of influenza C virus. Viruses 12, 1.

Shuai, L., et al., 2021. Replication, pathogenicity, and transmission of SARS-CoV-2 in minks. Natl. Sci. Rev. 8 (3), nwaa291.

Sun, W., et al., A Newcastle disease virus (NDV) expressing membrane-anchored spike as a cost-effective 2 inactivated SARS-CoV-2 vaccine. bioRxiv, 2020a.

Sun, W., et al., 2020b. Newcastle disease virus (NDV) expressing the spike protein of SARS-CoV-2 as a live virus vaccine candidate. EBioMedicine 62, 103132.

Sun, W., et al., 2021b. A Newcastle disease virus expressing a stabilized spike protein of SARS-CoV-2 induces protective immune responses. Nat. Commun. 12 (1), 6197.

Sun, Y., et al., Dual roles of a novel oncolytic viral vector-based SARS-CoV-2 vaccine: preventing COVID-19 and treating tumor progression. 2021a.

Wang, J., et al., 2021. Mucosal priming with a recombinant influenza A virus-vectored vaccine elicits T-cell and antibody responses to HIV-1 in mice. J. Virol. 95, 12.

Wang, M., Veit, M., 2016. Hemagglutinin-esterase-fusion (HEF) protein of influenza C virus. Protein Cell 7 (1), 28–45.

Wu, R., et al., 2010. A live bivalent influenza vaccine based on a H9N2 virus strain. Vaccine 28 (3), 673–680.

Yahalom-Ronen, Y., et al., 2020. A single dose of recombinant VSV-G-spike vaccine provides protection against SARS-CoV-2 challenge. Nat. Commun. 11 (1), 6402.

Yang, J., et al., 2017. Pathogenicity of modified bat influenza virus with different M genes and its reassortment potential with swine influenza A virus. J. Gen. Virol. 98 (4), 577–584.

Zhao, L., 2022. DDX5/METTL3-METTL14/YTHDF2 axis regulates replication of influenza A virus. Microbiol Spectr., e0109822

Zheng, A., 2020. Enhancing neuraminidase immunogenicity of influenza A viruses by rewiring RNA packaging signals. J. Virol. 94, 16.